



Article

Study on the Mechanical Properties of Silty Clay Sediments with Nodular Hydrate Occurrence

Cheng Lu ^{1,2,†}, Pengfei Xie ^{3,4,†}, Hui Li ^{3,5}, Xuhui Zhang ^{3,5,*} , Xiaobing Lu ^{3,5}, Bin Zhang ⁴ , Ziqin Zhang ⁴, Xuwen Qin ^{2,6}, Shuai Zhang ¹ and Hang Bian ^{1,4}

¹ Center of Oil & Natural Gas Resource Exploration, China Geological Survey, Beijing 100083, China; jaluch@126.com (C.L.); zhangshuai870517@163.com (S.Z.); bianhang1994@foxmail.com (H.B.)

² Guangzhou Marine Geological Survey, China Geological Survey, Guangzhou 510075, China; qinxuwen@163.com

³ Institute of Mechanics, Chinese Academy of Sciences, Beijing 100190, China; xpf970826@gmail.com (P.X.); lihui@imech.ac.cn (H.L.); xblu@imech.ac.cn (X.L.)

⁴ School of Engineering and Technology, China University of Geosciences (Beijing), Beijing 100083, China; sc_zhb@cugb.edu.cn (B.Z.); ark869182533@163.com (Z.Z.)

⁵ School of Engineering Science, University of Chinese Academy of Sciences, Beijing 100049, China

⁶ Department of Gas Hydrate, China Geological Survey, Beijing 100037, China

* Correspondence: zhangxuhui@imech.ac.cn

† These authors contributed equally to this work.

Abstract: Natural gas hydrates are a strategic energy resource in China. The China Geological Survey has discovered segregated hydrate mass formations under the seepage mechanism in the South China Sea through exploration, and gas hydrates occur in nodular, massive, and vein formations in silty clay sediment. Previous work has focused on the analysis of sediment mechanical properties with respect to the uniform distribution of natural gas hydrates in pore spaces, but the mechanical properties of hydrate-bearing sediments containing segregated hydrate masses are not well understood. Spherical hydrates are used to characterize nodular hydrates, a method is proposed for the preparation of sediment samples containing segregated hydrates masses, and a series of triaxial compression tests are carried out on the samples containing spherical hydrates with two kinds of particle sizes at a certain volume fraction. The paper presents triaxial stress–strain curves for the samples containing spherical hydrates. A model for predicting elastic modulus is established. The results present two distinct stages in the triaxial compression tests of silty clay sediments containing spherical hydrates; they also show that the elastic moduli predicted by the model are in good agreement with the experimental results when the model parameters are set at $\alpha = 0.5$ and $\beta = -0.21$. These results provide fundamental mechanical parameters for the safety evaluation of strata containing segregated gas hydrates.

Keywords: segregated gas hydrate mass; silty clay sediment; volume fraction; stress–strain curve



Citation: Lu, C.; Xie, P.; Li, H.; Zhang, X.; Lu, X.; Zhang, B.; Zhang, Z.; Qin, X.; Zhang, S.; Bian, H. Study on the Mechanical Properties of Silty Clay Sediments with Nodular Hydrate Occurrence. *J. Mar. Sci. Eng.* **2022**, *10*, 1059. <https://doi.org/10.3390/jmse10081059>

Academic Editor: Timothy S. Collett

Received: 4 July 2022

Accepted: 30 July 2022

Published: 1 August 2022

Publisher's Note: MDPI stays neutral with regard to jurisdictional claims in published maps and institutional affiliations.



Copyright: © 2022 by the authors. Licensee MDPI, Basel, Switzerland. This article is an open access article distributed under the terms and conditions of the Creative Commons Attribution (CC BY) license (<https://creativecommons.org/licenses/by/4.0/>).

1. Introduction

As a new clean energy resource, natural gas hydrates (GHs) have attracted considerable attention due to their wide distribution and large reserves [1,2]. In GH exploitation, the disruption of GH phase equilibrium due to depressurization and heat injection leads to dissociation and phase transition from solid to gas and water, decreasing the mechanical properties of sediments [3], and improper protection may lead to submarine geological hazards or alter the hydrological risks of cold regions, even the leakage of methane gas [4]. Hence, before the large-scale commercial exploitation of GH, it is necessary to predict the instabilities of strata in the process of exploitation. The accurate evaluation of the mechanical properties of hydrate-bearing sediments (HBSs) is of great importance.

The main method to obtain the mechanical properties of HBSs is to conduct laboratory tests on reconstructed samples, and theoretical constitutive models are presented according

to different assumptions and the characteristics of stress–strain curves. Laboratory tests mainly focus on high-pressure, low-temperature GH triaxial shear tests to obtain static and dynamic mechanical properties [5]. Winters et al. [6–8] used resonance and triaxial test methods to test in situ core samples and synthetic samples to obtain the strength and compression wave velocity of HBSs. Clayton et al. [9] tested the responses of hydrate-bearing sandy sediments under small strain loadings and found that the shear modulus of sediments is greatly improved when hydrates in cemented states act on sandy sediments. Hyodo et al. [10] found that the influence of hydrates on the mechanical properties of sand sediments depended on temperature, effective confining pressure, and GH saturation by triaxial tests on HBSs. Masui et al. [11] compared undisturbed samples and reconstructed samples and found that these samples have similar mechanical shear strengths but that the stress–strain relationships vary with initial porosity and grain size distribution. Previous studies [12–15] proved the similarity of mechanical properties between tetrahydrofuran (THF) hydrates and methane hydrates by laboratory tests. Lee et al. [16] synthesized HBS samples by THF and investigated how vertical effective stress, stress history, porosity, hydrate saturation, component composition, pore fluid ion concentration, and temperature affect the electromagnetic and mechanical properties of HBSs by a series of consolidation compression tests. Zhang et al. [17,18] conducted triaxial tests on synthesized THF hydrate-bearing sediments and found that the strength and deformation of the samples were obviously affected by particle size.

Limited by exploitation technology, it was believed that the exploitation of hydrates in sandy sediment reservoirs with higher porosities and permeabilities was the preferred scheme, and testing was mainly based on HBSs synthesized from sandy sediment [19]. However, a lot of hydrates are found in fine-grained sediments on the sea floor [20]. In sandy sediments, hydrates occur in the form of pore distributions and are approximately homogeneously distributed macroscopically. The occurrences are commonly in the particle-filling mode, particle-support mode, and cementation mode [21], as shown in Figure 1. However, in shallow, fine-grained sediments, hydrates occur in the form of segregated masses, such as nodular, veined, massive forms, etc. [22–24], as shown in Figure 2. The occurrences state of hydrates in sediments can be divided into two types: segregated (including fracture-filling, veined, nodular, thick-layer, etc., and the hydrates are heterogeneously distributed macroscopically) and pore type (including pore-filling, cementation, particle wrapping, skeleton-support, local aggregation, etc., and the hydrates are approximately homogeneously distributed macroscopically) [25]. The different occurrences of hydrates lead to great differences in the mechanical properties, such as the mechanical behavior and permeability, of sediments. Disturbance after hydrate dissociation and phase transformation may introduce local severe decreases in the mechanical properties of sediments in silt clay sediments. Inherent difficulties in hydrate formation hinder laboratory studies, which are thus limited to geophysical logs and numerical simulations and neglect the effects of hydrate formation on surrounding sediments [26,27]. Some scholars have also carried out preliminary explorations based on the synthesis of segregated hydrates from argillaceous clayey-silt sediments in the Shenhu Sea, but the preparation method of samples is incapable of controlling hydrate morphology [28].

Theoretical models play an important role in evaluating the mechanical response of strata and production in the process of hydrate production. Some scholars have established geophysical–geothermal schemes to quantify the saturation of the co-existing phases and predict phase the behavior of hydrates [29,30]. Moreover, scholars [31–39] have established mechanical models of HBSs based on traditional soil constitutive models. However, unlike the traditional geotechnical sediments, HBSs consist of a sediment skeleton, water, gas, and hydrates. Therefore, the constitutive model of HBS needs to consider the influence of hydrate saturation, occurrence mode, dissociation, and phase transformation on the mechanical properties of sediments. Zhang et al. [40] constructed a two-phase elastic medium model of HBS based on the rule of mixture of composites. The upper and lower limits for the elastic modulus of HBSs were expressed using parallel and series elements and by intro-

ducing the volume fraction of the sediment phase and the hydrate phase. Liang et al. [41] established an elastoplastic constitutive model of gas hydrate-bearing sediments based on homogenization theory. Hydrate crystals are regarded as an inclusion phase in the sediments, and the equivalent elastoplastic stiffness matrix of HBSs was derived. However, these models were based on the occurrence characteristics and experimental data for hydrates in the pores of hydrate-bearing sandy sediments, without considering the influence of factors such as segregated hydrate mass in silt clay sediments.

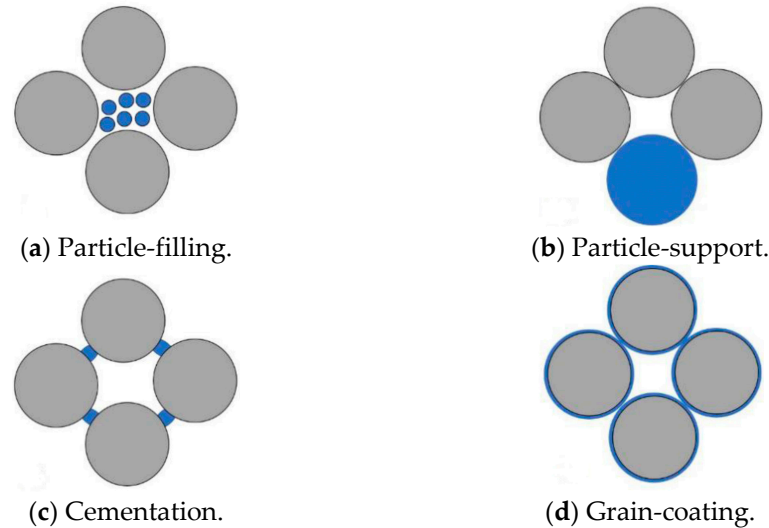


Figure 1. Hydrate occurrence modes of coarse-grained sediments [21].

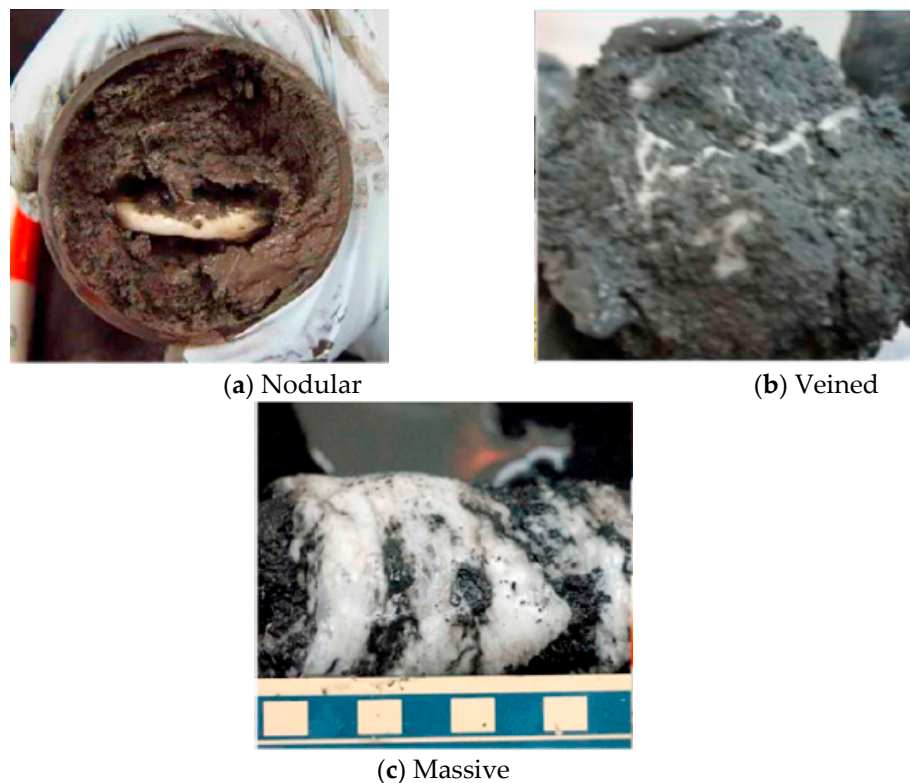


Figure 2. Hydrate occurrence modes in fine-grained sediments [22].

In this paper, the preparation method of test samples of sediments containing natural gas hydrates was improved to simulate the segregated hydrate mass in fine-grained sediments. Characterizations of nodular hydrates in reservoir by spherical hydrate and a series of triaxial tests were carried out to obtain stress–strain curves and modulus parameters of

HBS. The two-phase elastic modulus model of HBS was presented to describe the main feature of silty clay sediments containing spherical segregated hydrates.

2. Materials and Methods

The silty clay sediments from the GH zone in China were selected as the soil skeleton of the sample preparation. Hydrate occurrence is dominated by segregated states, such as nodular, massive, and veined states. In order to simulate the occurrence of GH, spherical hydrates were mixed in silty clay sediments using a new reconstructed HBS method, and the effect of spherical hydrates on the mechanical properties of sediments was investigated using the triaxial test.

2.1. Soil Skeleton Materials and Experimental Set-Up

The silty clay sediments used in the experiment were taken from the hydrate reservoirs in the South China Sea. The water depth was about 1000 m, and the hydrates occurred in the Quaternary sediments within a range of 7–160 m below the seafloor. The basic physical properties of the sediments were as follows: specific gravity of soil particles $G_S = 2.69$, the porosity was 0.52, and the dry bulk density was 1.3 g/cm^3 ; the particle size $d_{60} = 0.0131 \text{ mm}$, of which the clayey fraction ($d \leq 4 \mu\text{m}$) accounted for about 37% and the sandy fraction ($4 \mu\text{m} < d \leq 63 \mu\text{m}$) for about 51%, and the particle size distribution (PSD) curve is shown in Figure 3.

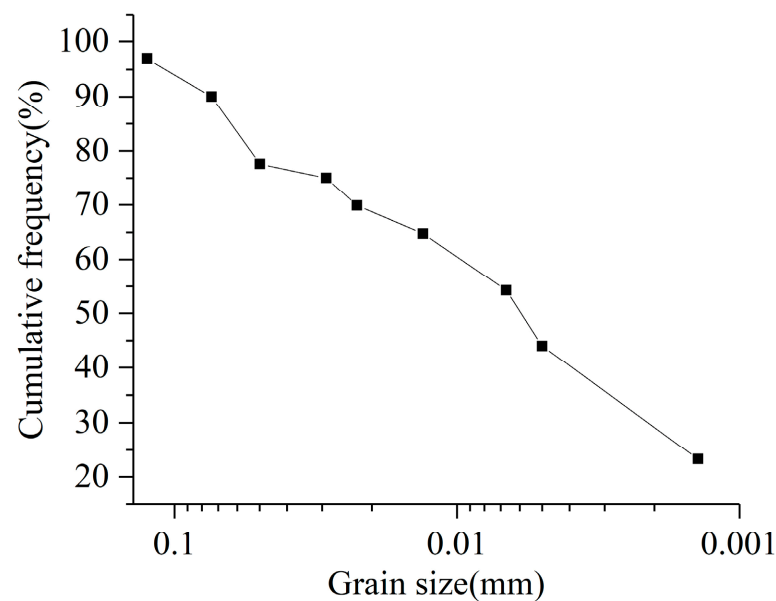


Figure 3. Particle size distribution (PSD) curve.

The engineering classification of the test soil: particles with a particle size of less than 0.075 mm have a mass of more than 50%, belonging to fine-grained soil; the nonuniform coefficient $C_u = \frac{d_{60}}{d_{10}} = 15.6$, so it was nonuniform; the curvature coefficient $C_c = \frac{d_{30}^2}{d_{60} \cdot d_{10}} = 0.55$, so the grading was discontinuous; the test soil was a fine-grained soil with poor grading.

The water saturation S_r was above 70%, the natural moisture content was about 30%, and the plasticity limit was about 30%.

Hydrates were prepared by mixing distilled water with a 99.9% concentration of tetrahydrofuran solution to form a solution with a mass fraction of 19%, which was cooled to synthesize THF hydrates at atmospheric pressure.

The high-pressure and low-temperature triaxial test system for HBSs of the Institute of Mechanics, Chinese Academy of Sciences, was adopted, as shown in Figure 4 [42]. The sample is placed in the pressure chamber, the confining pressure (σ_3) is provided by the pump, the longitudinal load ($\sigma_1 - \sigma_3$) is provided by the loading device, test data can be

recorded by the stress–strain monitor, and the whole system is placed in the incubator, which provides a low temperature. The temperature range of the incubator is $-20\text{ }^{\circ}\text{C}$ to $30\text{ }^{\circ}\text{C}$, which could be set at a constant value during tests ($\pm 0.5\text{ }^{\circ}\text{C}$). The pump can provide a maximum confining pressure of 14 MPa. The sample size has a diameter of 39.1 mm \times a length of 80 mm , and the dry bulk density of the sample is $\rho_d = 1.3\text{ g/cm}^3$.

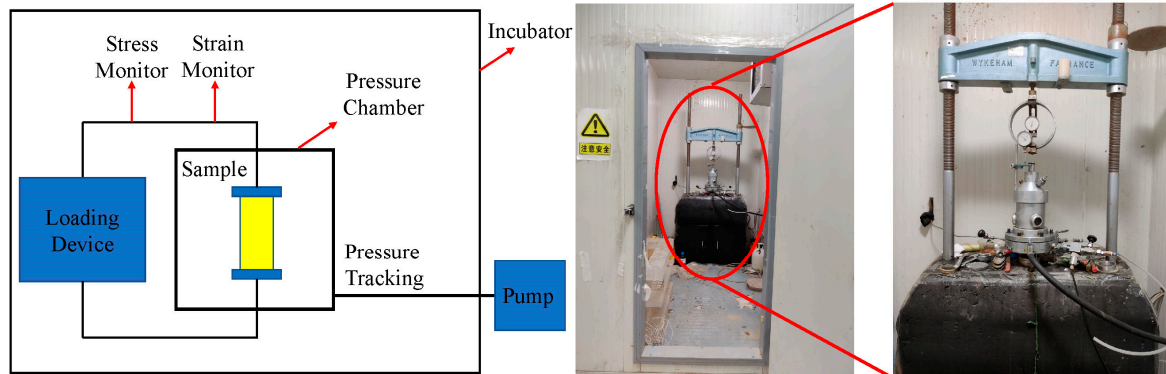


Figure 4. Schematic diagram and photo of the high-pressure and low-temperature triaxial test apparatus.

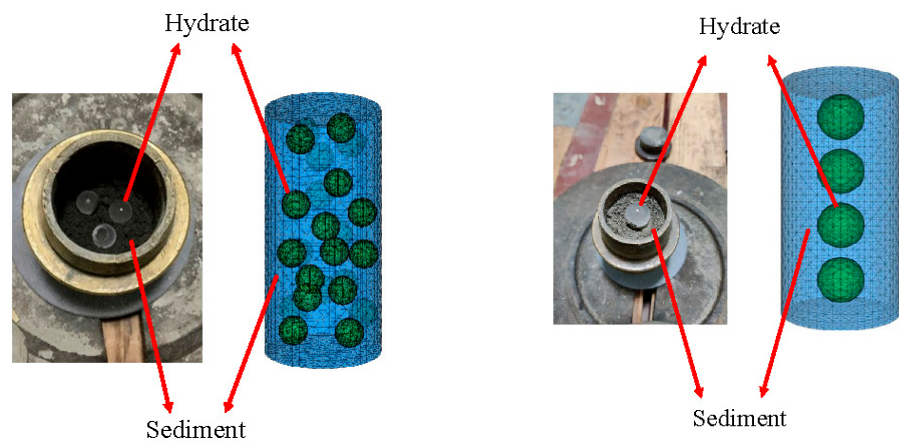
2.2. The Sample Preparation Method Containing Segregated Hydrate Masses

To reconstruct sediment samples containing segregated hydrate masses, the traditional HBS triaxial test sample preparation method was improved by pre-synthesizing hydrates and introducing them into sediments during the production of cylindrical test samples. Previous studies have obtained a phase equilibrium temperature of the THF solution, at $4.4\text{ }^{\circ}\text{C}$ standard atmospheric pressure, THF solution with mass fraction of 19% can fully synthesize hydrate. Moreover, the thermal conductivity, specific heat, bulk density, and mechanical properties of tetrahydrofuran (THF) hydrate and methane hydrate are similar, so THF was used to replace methane to synthesize the hydrates [28].

HBS samples were prepared by adding spherical hydrates during the process of compacting wet sediment into samples by layers under a low temperature to keep them undissociated. The wet sediment was prepared by using a spray to add distilled water into dry sediment particles and ensuring that the water content reached $\omega = 30\%$. The mass of the wet sediment was calculated as follows: $m_s = V \cdot \rho_d \cdot \omega$. The spherical hydrates were synthesized by pre-configuring THF solution with a mass fraction of 23% (to eliminate the error of tetrahydrofuran volatilization) into a sealed container and cooling it down.

Due to the particularity of segregated hydrate occurrence, the concept of hydrate saturation cannot be used to describe hydrate content; hence, a new definition, the hydrate volume fraction, $\nu = \frac{V_h}{V}$, was used. A standard size mold was used in this test, with a sample volume of $V = 96060\text{ mm}^3$. The volume of hydrates was controlled according to the diameter and number of formed spherical hydrates. The hydrate volume was $V_h = n \cdot \frac{4}{3} \cdot \pi \cdot r^3$, where n is the hydrate mass and r is the radius of the spherical hydrate.

Considering the low permeability of the silty clay samples and the quasi-static loading process, the triaxial unconsolidation undrained (UU) test was conducted by applying an axial compression rate of 0.8 mm/min , and the test was stopped when an engineering strain of 15% was reached. First, the same method was used to obtain the reference mechanical properties of sediment without hydrates. In the tests, spherical hydrates with radii of 8.5 mm and 5 mm were used to explore the influence of nodular hydrate size on the mechanical properties of HBSs, as shown in Figure 5. UU tests were carried out under different confining pressures, from 1 MPa – 5 MPa . The volume fraction of hydrate was about 11%, and the same volume was 10 cm^3 in each sample.



(a) Spherical hydrates with a radius of 8.5 mm (b) Spherical hydrates with a radius of 5 mm

Figure 5. Test sample and model diagram.

3. Results and Discussion

3.1. Stress–Strain Relationships

Triaxial test results for the sediments without hydrate samples are shown in Figure 6. With increase in confining pressure, the failure strengths and elastic moduli of the sediments gradually increased and gradually transformed from strain softening to strain hardening. According to the Mohr–Coulomb criterion, the strength envelopes of the sediments were drawn, as shown in Figure 7. The sediment cohesion $c = 110$ kPa and the angle of internal friction $\varphi = 2^\circ$. It is noted that the red trend lines of all the stress–strain curves give a direct indication of whether the mechanical behavior of the specimen in question is elastic, perfectly plastic, strain hardening, or strain softening.

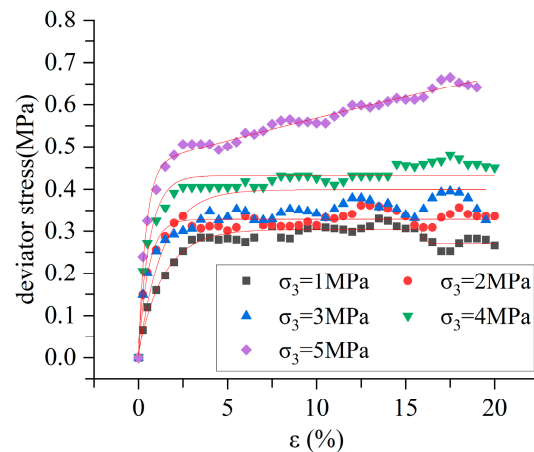


Figure 6. Triaxial stress–strain curves of sediments.

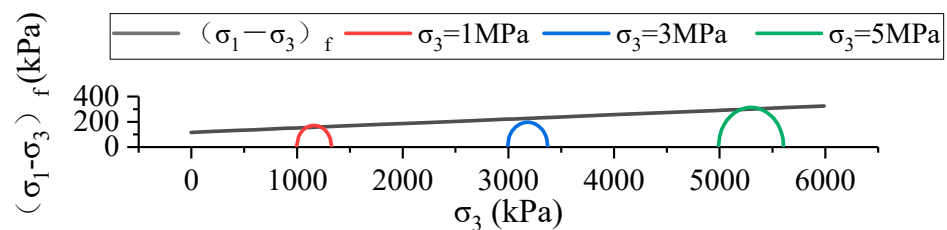


Figure 7. Sediment strength envelope diagram.

The triaxial test results for the silty clay samples containing spherical hydrates ($r = 5$ mm) are shown in Figure 8. The mechanical properties of the samples were significantly enhanced. In the triaxial test, the failure strength and elastic modulus of HBSs increased with

the increase in confining pressure but decreased under the test conditions of confining pressures greater than 3 MPa. Different from the conventional elastoplastic deformation characteristics of sandy sediments with homogeneous hydrates, the triaxial stress–strain curves of clay sediments containing spherical hydrates can be roughly divided into two stages: (I) an elastic phase, in which the deviator stress of the sample increases rapidly in the small strain range ($\epsilon \leq 1\%$) and the deviator stress ($\sigma_1 - \sigma_3$) of the sample has reached more than 50% of the failure strength when $\epsilon = 1\%$; (II) when the strain $\epsilon > 1\%$, the sample enters into a plastic phase, in which the deviator stress no longer changes significantly.

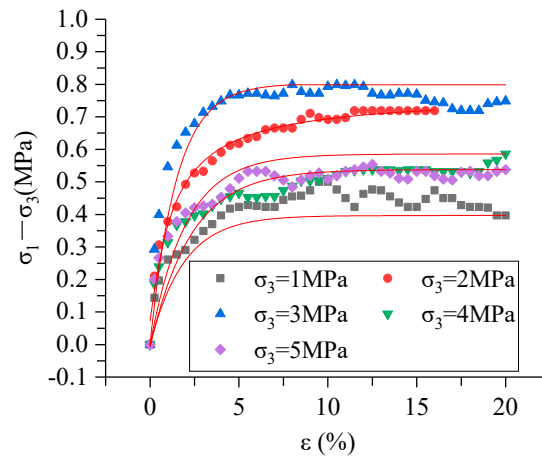


Figure 8. Triaxial stress–strain curves of sediments containing spherical hydrates ($r = 5$ mm).

Under the same experimental conditions, the results for the sediment samples containing spherical hydrates ($r = 8.5$ mm) are shown in Figure 9. With the increase in hydrate radius, the mechanical properties of the samples improved, while the curve trends are similar to those of the sediments containing spherical hydrates ($r = 5$ mm). When the confining pressure was greater than 3 MPa, the mechanical properties of the samples in this test also decrease. The reason may be local stress concentrations caused by spherical hydrate occurrence in sediments. According to Saint-Venant’s Principle, the range of local stress concentrations is twice the diameter of spherical hydrates, and they overlap as shown in Figure 10. Under the condition of high confining pressure, the overlapping range of local stress concentrations may lead to the formation of micro-fractures in sediments, resulting in a decrease in the strength of samples.

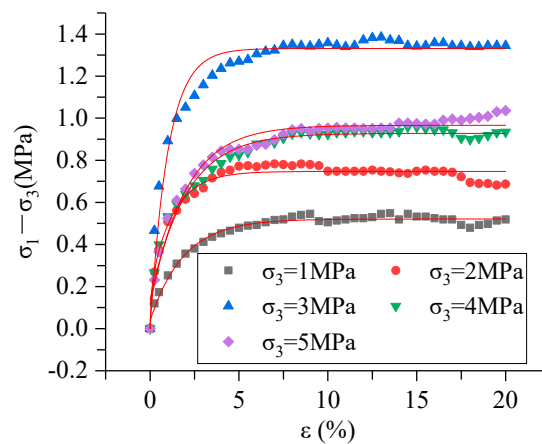


Figure 9. Triaxial stress–strain curves of sediments containing spherical hydrates ($r = 8.5$ mm).

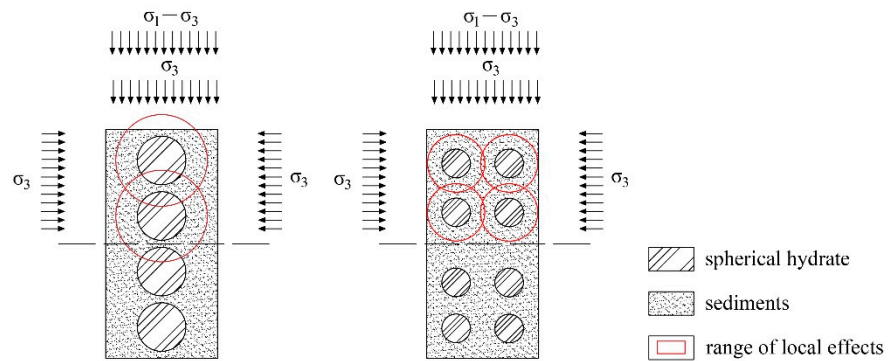


Figure 10. Stress analysis diagrams of the samples.

The experimental condition involving spherical hydrates ($r = 5 \text{ mm}$) and a confining pressure of 3 MPa was selected as an example to compare reductions in the shear strength of HBS before and after hydrate dissociation, as shown in Figure 10. After spherical hydrate dissociation, the failure strength of sediments decreased from 0.8 MPa to 0.33 MPa, and the reduction was more than 50%, as shown in Figure 11.

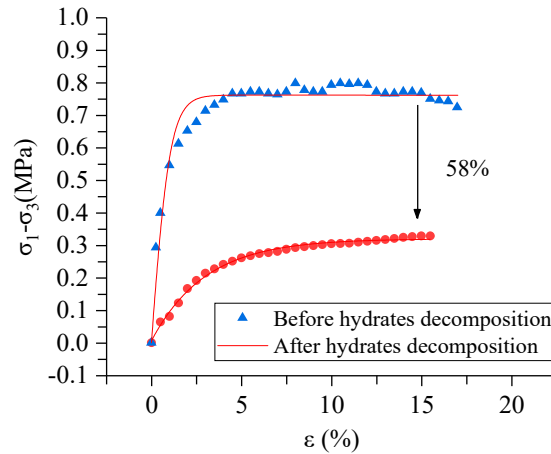


Figure 11. Comparison of HBS shear strength before and after hydrate dissociation.

3.2. Discussion of the Modulus

The triaxial test results show that when the confining pressure is less than 3 MPa, the elastic modulus of sediment containing spherical hydrates increases with the increase in confining pressure, but the elastic modulus decreases once the confining pressure is greater than 3 MPa, which may be related to the size effect of internal defects under high confining pressures. The results of different tests with a confining pressure of less than 3 MPa were selected for the fitting of the model parameters. The triaxial test results of sediments without hydrates are shown in Figure 6. The secant modulus was selected to replace the elastic modulus, and the secant modulus E_{50} of the test samples under various confining pressures is shown in Table 1.

Table 1. Secant modulus for sediments without hydrates.

| Confining pressure (MPa) | 1 | 2 | 3 |
|--------------------------|----|----|----|
| Secant modulus (MPa) | 16 | 32 | 45 |

In the triaxial test results for HBSs, the secant modulus E_{50} was also selected as the elastic modulus of the test sample, as shown in Tables 2 and 3. The elastic modulus of the hydrates was 9 GPa [15,43].

Table 2. Secant modulus of sediments containing spherical hydrates ($r = 5$ mm).

| | | | |
|---------------------------------|----|----|----|
| Confining pressure (MPa) | 1 | 2 | 3 |
| Secant modulus (MPa) | 26 | 42 | 80 |

Table 3. Secant modulus of sediments containing spherical hydrates ($r = 8.5$ mm).

| | | | |
|---------------------------------|----|----|-----|
| Confining pressure (MPa) | 1 | 2 | 3 |
| Secant modulus (MPa) | 39 | 76 | 136 |

3.3. Theoretical Expressions for the Moduli of Two-Phase Composites

Sediments containing spherical hydrates can be regarded as four-phase composite materials containing sediment skeletons, hydrates, pore gas, and pore water. Since pore fluid (water, gas) cannot bear shear deformation, sediments containing spherical hydrates are simplified as two-phase composites. The silty clay sediments containing pores are regarded as the matrix, and the spherical hydrate mass is regarded as a reinforcement phase. The strengthening effect depends on the mechanical properties, contents, the shape of the reinforcement phase, and the contact mode of each phase. In the test cases, it is determined mainly by the volume fraction and diameter of the spherical hydrate.

Zhang et al. constructed a Two-Phase Elastic Modulus model based on the Composite Mixing Law to predict the equivalent elastic modulus of composites. Each HBS unit consists of four sub-units and each sub-unit is composed of series-parallel modes, as shown in Figure 12 [40].

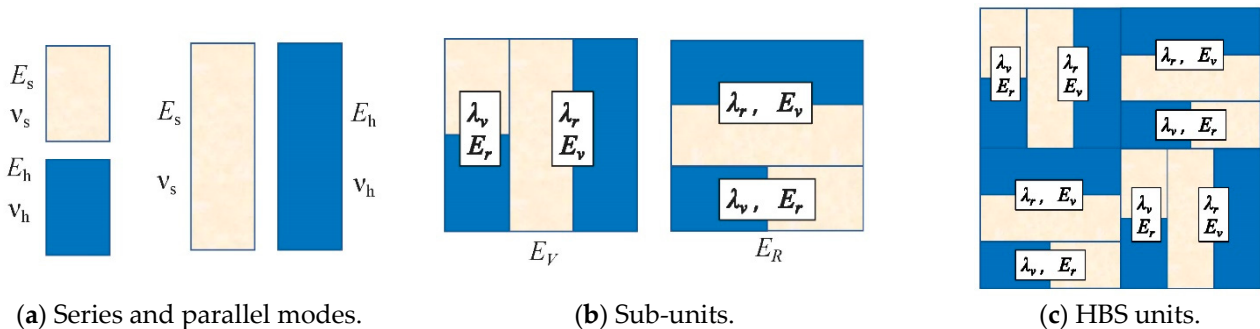


Figure 12. Two-phase elastic modulus model diagram.

Under the condition of compression deformation, there are two transmission paths in series and parallel. According to the assumption of equal stress in the series model:

$$E_r = \left(\frac{V_1}{E_1} + \frac{V_2}{E_2} \right)^{-1},$$

and according to the assumption of equal strain in the parallel model:

$$E_v = E_1 \cdot V_1 + E_2 \cdot V_2,$$

where V_1 is the volume fraction of sediments in the sample and V_2 is the volume fraction of hydrates, satisfying $V_1 + V_2 = 1$; E_1 is the elastic modulus of sediments and E_2 is the elastic modulus of hydrates.

The introduction of the microscopic parameters λ_v and λ_r represents the influence degrees of the series and parallel structures on the elements, respectively:

$$E_V = E_v \cdot \lambda_r + E_r \cdot \lambda_v,$$

$$E_R = \left(\frac{\lambda_r}{E_r} + \frac{\lambda_v}{E_v} \right)^{-1}.$$

The expression for the equivalent modulus of elasticity:

$$E_{eff} = \left[\frac{1}{2} \left(\frac{\lambda_r}{E_r} + \frac{\lambda_v}{E_v} \right) + \frac{\frac{1}{2}}{\lambda_r E_v + \lambda_v E_r} \right]^{-1}$$

is obtained by the central symmetry. By differentiating the unknown quantities λ_v, λ_r according to the Lagrange limit method and associating the control conditions $\lambda_v, \lambda_r \geq 0, \lambda_v + \lambda_r = 1$, the upper and lower limits of the equivalent elastic modulus are obtained:

- (1) When $\frac{\lambda_v}{\lambda_r} = \left(\frac{E_v}{E_r}\right)^{\frac{1}{2}}$, this elastic modulus is the upper limit:

$$E_{max} = \sqrt{E_v \cdot E_r};$$

- (2) When $\lambda_v \times \lambda_r = 0$, this elastic modulus is the low limit:

$$E_{min} = \frac{2E_v \cdot E_r}{E_v + E_r}.$$

The theoretical model takes into account the effect of interphase interaction on the basis of the mixing theory. Even when the elastic moduli of the reinforced phase and the matrix are quite different, the upper and lower limits of the equivalent elastic modulus can be well predicted.

In this study, segregated spherical hydrates were used. The interaction between hydrates and sediments was related to the diameter and volume fraction of hydrates and the confining pressure. Furthermore, the influence degree of series and parallel structures on elements was related to the confining pressure, for hydrates are segregated in sediments without cement. Therefore, confining pressure should be introduced into the expressions of λ_r :

$$\lambda_r = e^{(\beta \cdot \frac{E_1}{E_0})},$$

$$\lambda_v = 1 - \lambda_r,$$

and with the introduction of the dimensionless quantity $\alpha \cdot \left(\frac{r}{r_0}\right)$, the modified equivalent elastic modulus expression is:

$$E = \frac{\alpha \cdot \frac{r}{r_0}}{\left[\frac{1}{2} \left(\frac{e^{(\beta \cdot \frac{E_1}{E_0})}}{E_r} + \frac{1 - e^{(\beta \cdot \frac{E_1}{E_0})}}{E_v} \right) + \frac{\frac{1}{2}}{(e^{(\beta \cdot \frac{E_1}{E_0})}) \cdot E_v + (1 - e^{(\beta \cdot \frac{E_1}{E_0})}) E_r} \right]}$$

where E_1 is the elastic modulus of the silty clay sediments at different confining pressures, which is used as the independent variable in this equation; E_0 is the elastic modulus of the sediment at a confining pressure of 1 MPa, which forms a dimensionless quantity $\frac{E_1}{E_0}$ with E_1 ; the elastic modulus of hydrates is selected as $E_2 = 9000$ MPa, according to a previous study; r_1 is the radius of the spherical hydrates and forms a dimensionless quantity $\frac{r_1}{r_0}$ with the minimum spherical hydrate radius ($r_0 = 5$ mm) in this test; and α, β is a correction parameter, the values of which are given in Table 4.

Table 4. Values of fitting parameters.

| E_0 (MPa) | E_2 (MPa) | V_1 (%) | V_2 (%) | r_0 (mm) |
|-------------|-------------|-----------|-----------|------------|
| 16 | 9000 | 89 | 11 | 5 |

When α is taken as 0.5 and β is taken as -0.21 , the elastic modulus predicted by the model agrees well with that of the test results, as shown in Figure 13.

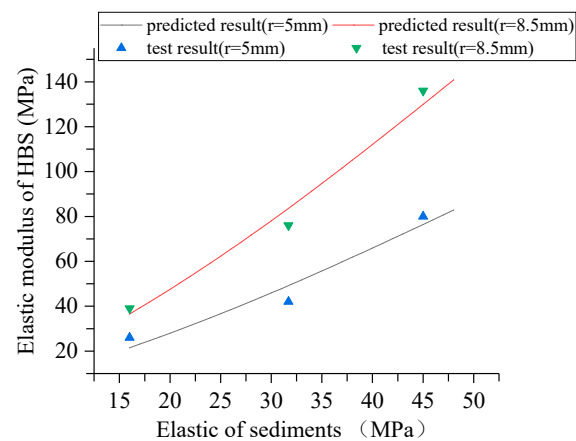


Figure 13. Comparison between test and theoretical results for elastic moduli.

4. Conclusions

A new reconstructed sample method for sediments with segregated hydrate mass has been presented, the concept of GH saturation redefined as volume fraction to describe the phase content, and a series of triaxial tests have been carried out. The heterogeneity of hydrates was characterized by changing the diameters of segregated hydrate masses. The results are as follows:

- (1) Different from the elastic–plastic stress–strain characteristics of sandy sediments containing homogeneous pore-filled hydrates, the triaxial stress–strain curves of the test samples have obvious elastic and plastic stages. Under the same hydrate volume fraction, with the increase in confining pressure, the strengths and elastic moduli of the test samples improved, and when the confining pressure exceeded 3 MPa, the shear strength decreased due to the fracturing effect under high pressure.
- (2) Based on the theory of composite mechanics, the two-phase elastic modulus model proposed by Zhang et al. was improved to describe the effect of the heterogeneity of hydrates. By comparing the theoretical results with the test results, it was found that when the value α was 0.5 and β was -0.21 , the elastic modulus predicted by the model agreed well with the test results.

Notably, the spherical hydrates studied in this paper are an ideal simulation of the nodular hydrates that naturally occur, and in future studies we hope to investigate scenarios of heterogeneous occurrence involving veined or fractured forms.

Author Contributions: Conceptualization, C.L., X.Z. and X.L.; methodology, P.X., H.L. and X.Z.; validation, C.L., S.Z., H.B. and X.Q.; formal analysis, C.L., P.X. and Z.Z.; investigation, P.X.; resources, C.L. and X.Q.; writing—original draft preparation, P.X. and H.L.; writing—review and editing, C.L., X.Z. and X.L.; supervision, B.Z. and X.Z.; project administration, C.L. and X.Z.; funding acquisition, C.L. and X.Q. All authors have read and agreed to the published version of the manuscript.

Funding: This research was funded by the China Geological Survey Project (no. DD20211350), the National Natural Science Foundation of China (51991365, 11872365), and the Guangdong Major Project of Basic and Applied Basic Research (no. 2020B0301030003).

Institutional Review Board Statement: Not applicable.

Informed Consent Statement: Not applicable.

Data Availability Statement: The data that support the findings of this study are available within the article.

Conflicts of Interest: The authors declare no conflict of interest.

References

1. Zhang, H.; Luo, X.; Bi, J.; He, G.; Guo, Z. Submarine slope stability analysis during natural gas hydrate dissociation. *Mar. Georesources Geotechnol.* **2019**, *37*, 467–476. [[CrossRef](#)]
2. Lijith, K.P.; Malagar, B.R.C.; Singh, D.N. A comprehensive re-view on the geomechanical properties of gas hydrate bearing sediments. *Mar. Pet. Geol.* **2019**, *104*, 270–285. [[CrossRef](#)]
3. Sloan, E.D. *Clathrate Hydrates of Natural Gases*, 2nd ed.; Revised and Expanded; The Chemical Rubber Company Press: Boca Raton, FL, USA, 1998.
4. Farahani, M.V.; Hassanpouryouzband, A.; Yang, J.; Tohidi, B. Insights Into the Climate-driven Evolution of Gas Hydrate-bearing Permafrost Sediments: Implications for Prediction of Environmental Impacts and Security of Energy in Cold Regions. *RSC Adv.* **2021**, *11*, 14334–14346. [[CrossRef](#)] [[PubMed](#)]
5. Hyodo, M.; Wu, Y.; Nakashima, K.; Kajiyama, S.; Nakata, Y. Influence of Fines Content on the Mechanical Behavior of Methane Hydrate-bearing Sediments. *J. Geophys. Res. Solid Earth* **2017**, *122*, 7511–7524. [[CrossRef](#)]
6. Winters, W.J.; Pecher, I.A.; Waite, W.; Mason, D.H. Physical Properties and Rock Physics Models of Sediment Containing Natural and Laboratory-formed Methane Gas Hydrate. *Am. Mineral.* **2004**, *89*, 1221–1227. [[CrossRef](#)]
7. Winters, W.; Waite, W.; Mason, D.; Gilbert, L.; Pecher, I. Methane Gas Hydrate Effect on Sediment Acoustic and Strength Properties. *J. Pet. Sci. Eng.* **2007**, *56*, 127–135. [[CrossRef](#)]
8. Winters, W.J.; Dallimore, S.R.; Collett, T.S.; Jenner, K.A.; Katsube, J.T.; Cranston, R.E.; Uchida, T. Relation between Gas Hydrate and Physical Properties at the Mallik 21–38 Research Well in the Mackenzie Delta. *Ann. N. Y. Acad. Sci.* **2010**, *912*, 94–100. [[CrossRef](#)]
9. Clayton, C.; Priest, J.A.; Best, A.I. The Effects of Disseminated Methane Hydrate on the Dynamic Stiffness and Damping of a Sand. *Géotechnique* **2005**, *55*, 423–434. [[CrossRef](#)]
10. Kajiyama, S.; Hyodo, M.; Nakata, Y.; Yoshimoto, N.; Wu, Y.; Kato, A. Shear Behaviour of Methane Hydrate-bearing Sand with various particle characteristics and fines. *Soils Found.* **2007**, *57*, 176–193. [[CrossRef](#)]
11. Masui, A.; Haneda, H.; Ogata, Y.; Aoki, K. Compaction behavior of Toyoura sand during methane hydrate dissociation. In Proceedings of the Seventh (2007) Isope Ocean Mining (& Gas Hydrates) Symposium, Lisbon, Portugal, 1–6 July 2007; pp. 53–56.
12. Yun, T.S.; Santamarina, J.C.; Ruppel, C. Mechanical Properties of Sand, Silt, and Clay Containing Tetrahydrofuran Hydrate. *J. Geophys. Res. -Solid Earth* **2007**, *112*. [[CrossRef](#)]
13. Nagashima, K.; Suzuki, T.; Nagamoto, M.; Shimizu, T. Formation of periodic layered pattern of tetrahydrofuran clathrate hydrates in porous media. *J. Phys. Chem. B* **2008**, *112*, 9876–9882. [[CrossRef](#)] [[PubMed](#)]
14. Zhang, X.H.; Wang, S.Y. Advances in Study of Mechanical Properties of Gas Hydrate-Bearing Sediments. *Open Ocean. Eng. J.* **2013**, *6*, 26–40.
15. Vlastic, T.M.; Servio, P.D.; Rey, A.D. THF Hydrates as Model Systems for Natural Gas Hydrates: Comparing Their Mechanical and Vibrational Properties. *Ind. Eng. Chem. Res.* **2019**, *58*, 16588–16596. [[CrossRef](#)]
16. Lee, J.Y.; Santamarina, J.C.; Ruppel, C. Mechanical and Electromagnetic Properties of Northern Gulf of Mexico Sediments with and without Thf Hydrates. *Mar. Pet. Geol.* **2008**, *25*, 884–895. [[CrossRef](#)]
17. Zhang, X.-H.; Lu, X.-B.; Zhang, L.-M.; Wang, S.-Y.; Li, Q.-P. Experimental Study on Mechanical Properties of Methane-hydrate-bearing Sediments. *Acta Mech. Sin.* **2012**, *28*, 1356–1366. [[CrossRef](#)]
18. Luo, T.; Song, Y.; Zhu, Y.; Liu, W.; Liu, Y.; Li, Y.; Wu, Z. Triaxial Experiments on the Mechanical Properties of Hydrate-bearing Marine Sediments of South China Sea. *Mar. Pet. Geol.* **2016**, *77*, 507–514. [[CrossRef](#)]
19. Wu, N.; Li, Y.; Wan, Y.; Sun, J.; Huang, L.; Mao, P. Prospect of marine natural gas hydrate stimulation theory and technology system. *Nat. Gas Ind.* **2020**, *40*, 100–115. [[CrossRef](#)]
20. Lei, L.; Santamarina, J.C. Laboratory Strategies for Hydrate Formation in Fine-grained Sediments. *J. Geophys. Res. Solid Earth* **2018**, *123*, 2583–2596. [[CrossRef](#)]
21. Lv, J.; Zhao, J.; Jiang, L.; Liu, Y.; Mu, H. A Review of Micro Computed Tomography Studies on the Gas Hydrate Pore Habits and Seepage Properties in Hydrate Bearing Sediments. *J. Nat. Gas Sci. Eng.* **2020**, *83*, 103555. [[CrossRef](#)]
22. Lei, L.; Santamarina, J.C. Physical properties of fine-grained sediments with segregated hydrate lenses. *Mar. Pet. Geol.* **2019**, *109*, 899–911. [[CrossRef](#)]
23. Liang, J.; Zhang, W.; Lu, J.A.; Wei, J.; Kuang, Z.; He, Y. Geological Occurrence and Accumulation Mechanism of Natural Gas Hydrates in the Eastern Qiongdongnan Basin of the South China Sea Insights From Site Gmgs5-w9-2018. *Mar. Geol.* **2019**, *418*, 106042. [[CrossRef](#)]
24. Ye, J.; Wei, J.; Liang, J.; Lu, J.; Lu, H.; Zhang, W. Complex Gas Hydrate System in a Gas Chimney, South China Sea. *Mar. Pet. Geol.* **2019**, *104*, 29–39. [[CrossRef](#)]
25. Ning, F.L.; Liang, J.Q.; Wu, N.Y.; Zhu, Y.H.; Wu, S.G.; Liu, C.L.; Ou, W.J. Reservoir characteristics of natural gas hydrates in China. *Nat. Gas Ind.* **2020**, *40*, 1–24, (In Chinese with English Abstract).
26. Ghosh, R.; Sain, K.; Ojha, M. Effective medium modeling of gas hydrate-filled fractures using the sonic log in the Krishna-Godavari basin, offshore eastern India. *Geophys. Res. Solid Earth* **2010**, *115*, B06101. [[CrossRef](#)]
27. Yun, T.S.; Lee, C.; Lee, J.S.; Bahk, J.J.; Santamarina, J.C. A pressure core based characterization of hydrate-bearing sediments in the Ulleung Basin, Sea of Japan (East Sea). *Geophys. Res. Solid Earth* **2011**, *116*, B02204. [[CrossRef](#)]

28. Li, Y.L.; Liu, C.L.; Liao, H.L.; Dong, L.; Bu, Q.; Liu, Z. Mechanical properties of the mixed system of clayey-silt sediments and natural gas hydrates. *Nat. Gas Ind.* **2020**, *40*, 159–168, (In Chinese with English Abstract).
29. Farahani, M.V.; Hassanpouryouzband, A.; Yang, J.; Tohidi, B. Development of a Coupled Geophysical-geothermal Scheme for Quantification of Hydrates in Gas Hydrate-bearing Permafrost Sediments. *Phys. Chem. Chem. Phys.* **2021**, *23*, 24249–24264. [[CrossRef](#)] [[PubMed](#)]
30. Hassanpouryouzband, A.; Joonaki, E.; Farahani, M.V.; Takeya, S.; Ruppel, C.; Yang, J.; Tohidi, B. Gas Hydrates in Sustainable Chemistry. *Chem. Soc. Rev.* **2020**, *49*, 5225–5309.
31. Yu, F.; Song, Y.; Li, Y.; Liu, W.; Lam, W. Analysis of Stress-strain Behavior and Constitutive Relation of Methane Hydrate-bearing Sediments with Various Porosity. *Int. J. Offshore Polar Eng.* **2011**, *21*, 316–322.
32. Yu, F.; Song, Y.; Liu, W.; Li, Y.; Lam, W. Analyses of Stress Strain Behavior and Constitutive Model of Artificial Methane Hydrate-Sciencedirect. *J. Pet. Sci. Eng.* **2011**, *77*, 183–188. [[CrossRef](#)]
33. Miyazaki, K.; Tenma, N.; Aoki, K.; Yamaguchi, T. A Nonlinear Elastic Model for Triaxial Compressive Properties of Artificial Methane-hydrate-bearing Sediment Samples. *Energies* **2012**, *5*, 4057–4075. [[CrossRef](#)]
34. Freij-Ayoub, R.; Tan, C.; Clennell, B.; Tohidi, B.; Yang, J. A Wellbore Stability Model for Hydrate Bearing Sediments. *J. Pet. Sci. Eng.* **2007**, *57*, 209–220. [[CrossRef](#)]
35. Klar, A.; Soga, K.; Ng, M. Coupled Deformation-flow Analysis for Methane Hydrate Extraction. *Géotechnique* **2010**, *60*, 765–776. [[CrossRef](#)]
36. Pinkert, S.; Grozic, J. An Analytical-experimental Investigation of Gas Hydrate-bearing Sediment Properties. In Proceedings of the Canadian Geotechnical Conference and the 11th Joint Cgs/iahcnc Ground Water Conference, Montreal, CA, USA, 29 September–3 October 2013.
37. Pinkert, S.; Grozic, J. Prediction of the Mechanical Response of Hydrate-bearing Sands. *J. Geophys. Res. Solid Earth* **2014**, *119*, 4695–4707. [[CrossRef](#)]
38. Uchida, S.; Soga, K.; Yamamoto, K. Critical State Soil Constitutive Model for Methane Hydrate Soil. *J. Geophys. Res. -Solid Earth* **2012**, *117*. [[CrossRef](#)]
39. Zhang, J.; Wang, Z.; Sun, B.; Sun, X.; Liao, Y. A constitutive model of hydrate bearing sediments in water-rich phase environments. *Chin. J. Undergr. Space Eng.* **2019**, *15* (Suppl. 2), 563–568.
40. Zhang, X.; Liu, L.-L.; Zhou, J.; Lu, X.; Wang, S.; Liu, C.; Ye, Y. Model for the Elastic Modulus of Hydrate-bearing Sediments. *Int. J. Offshore Polar Eng.* **2015**, *25*, 314–319. [[CrossRef](#)]
41. Liang, W.; Zhou, J.; Chen, P.; Wei, C. An elastoplastic constitutive model of gas hydrate bearing sediments based on homogenization theory. *Rock Soil Mech.* **2021**, *42*, 481–490, (In Chinese with English Abstract).
42. Wang, S.; Luo, D.; Zhang, X.; Lu, X.; Shi, Y. Experimental study of mechanical properties of hydrate clay. *J. Exp. Mech.* **2018**, *33*, 245–252. Available online: <https://mall.cnki.net/magazine/Article/SYLX201802010.htm> (accessed on 29 July 2022). (In Chinese with English Abstract).
43. Bathe, M.; Vagle, S.; Saunders, G.A.; Lambson, E.F. Ultrasonic Wave Velocities in the Structure Ii Clathrate Hydrate Thf·17h2o. *J. Mater. Sci. Lett.* **1984**, *3*, 904–906. [[CrossRef](#)]